NIH Public Access
Author Manuscript
Urology. Author manuscript; available in PMC 2013 January 03.

Published in final edited form as:
Urology. 2012 January ; 79(1): 233–239. doi:10.1016/j.urology.2011.10.002.

A Step Towards Personalized Medicine: Use of a Patient-Specific MRI based Prostate Mold for Validation of Multi-parametric MRI in the Localization of Prostate Cancer

Hari Trivedi, B.S.[a,*], **Baris Turkbey, M.D.**[b], **Ardeshir R. Rastinehad, D.O.**[c], **Compton J. Benjamin, M.D., Ph.D.**[c], **Marcelino Bernardo, B.S.**[b,d], **Thomas Pohida, M.S.**[e], **Vijay Shah, Ph.D.**[b,d], **Maria J. Merino, M.D.**[f], **Bradford J. Wood, M.D.**[a], **W. Marston Linehan, M.D.**[c], **Aradhana M. Venkatesan, M.D.**[a], **Peter L. Choyke, M.D.**[b], and **Peter A. Pinto, M.D.**[a,c]

[a]Center for Interventional Oncology, Radiology and Imaging Sciences CC, NCI, NIH, Bethesda, MD, USA

[b]Molecular Imaging Program, NCI, NIH, Bethesda, MD, USA

[c]Urologic Oncology Branch, NCI, NIH, Bethesda, MD, USA

[d]Imaging Physics, SAIC Frederick, Inc., NCI-Frederick, Frederick, MD, USA

[e]Division of Computational Bioscience, Center for Information Technology, NIH, Bethesda, MD, USA

[f]Laboratory of Pathology, NCI, NIH, Bethesda, MD, USA

Keywords

prostate cancer; patient-specific mold; multiparametric MRI; registration; correlation

Introduction

Prostate cancer is the second most common cancer in men (after skin cancer) as well as the second most common cause of cancer death (after lung cancer). In 2010, it is estimated that there will be 217,730 new cases diagnosed and approximately 32,050 deaths.[1] Over the last decade, there has been a steady rise in the detection of prostate cancer largely due to increased use of prostate-specific antigen (PSA) screening. This has led to increased use of systematic transrectal ultrasound (TRUS) guided biopsy in which the prostate is sampled in the same stereotypical fashion in all patients regardless of tumor location, resulting in false negatives in 10–40% of cases.[2–5] Advanced imaging techniques, primarily magnetic resonance imaging (MRI) have the potential to address this by allowing more accurate tumor localization, enabling image-guided targeted biopsies[6] as well as facilitating optimal planning of treatment. This will prove to be especially useful with the emergence of novel and potentially less morbid targeted therapies.[7]

T2-weighted (T2W) MR imaging has traditionally been used for morphologic prostate cancer imaging, however it is limited by its low specificity particularly in the central gland. Even in the peripheral zone, benign conditions such as prostatitis, benign prostatic

Address correspondence to: Peter A. Pinto M.D., Urologic Oncology Branch, National Cancer Institute, 10 Center Dr., MSC 1210, Bldg 10, Room 2-5940, Bethesda, MD 20892-1088, Telephone: 301-496-6353, Fax: 301-402-0922, pintop@mail.nih.gov.

*This research year was made possible through the Clinical Research Training Program, a public-private partnership supported jointly by the NIH and Pfizer Inc (via a grant to the Foundation for NIH from Pfizer Inc).

$watermark-text
$watermark-text
$watermark-text

$watermark-text

$watermark-text

$watermark-text

hyperplasia (BPH), or scarring can appear hypointense on T2-weighted MRI, mimicking cancer. To overcome this, additional techniques such as MR spectroscopy (MRS), dynamic contrast enhanced (DCE) MRI, and diffusion-weighted MR imaging (DW MRI) have been used to increase specificity with improved results.[8–13] Areas suspicious for prostate cancer have an increased choline (cho) to citrate (cit) ratio on MRS, increased early contrast uptake and washout on DCE MRI, and a hypointense appearance indicative of decreased Brownian motion of water on DW MRI. However, implementing these sequences requires more time, higher signal-to-noise ratios (SNR), and higher field strength magnets.[14–15]

Despite these advances in multiparametric MR imaging, a major obstacle in validation of MRI remains the accurate registration of whole-mount histopathology slices to imaging findings. Previous papers, including our prior work, have addressed this issue with numerous techniques for registration and slicing.[14,16–21]

To accurately register whole mount histopathology to MRI, we previously described a technique to create a patient-specific MRI-based prostate mold[22]. The one-to-one correlation between histopathology and MRI findings enables reliable reporting of the accuracy of multiparametric MRI for localization of prostate cancer. Herein, we describe the application of our customized mold to a patient with prostate cancer, and present the resultant correlation of MRI findings with histopathology sections.

Case Presentation

A 67-year old man presented to his local urologist for yearly PSA screening and digital rectal exam (DRE). He had lower urinary tract symptoms including weak urinary stream and incomplete emptying. Serum PSA was elevated to 5.6 ng/mL. A TRUS guided biopsy was performed which revealed Gleason 6 (3+3) prostatic adenocarcinoma in 2 of 12 cores (8% in the left lateral mid, 6% in the right lateral mid). The patient's American Urologic Association Symptom Score (AUASS) was 17 out of 35 and Sexual Health Inventory for Men (SHIM) score was 18 out of 25. Physical exam revealed a small palpable left apical prostate nodule on digital rectal examination but was otherwise unremarkable. Review of systems was negative.

The patient sought a second opinion and was seen in the NCI Multidisciplinary Prostate Cancer Clinic. After consultation he chose to undergo a multiparametric prostate MRI at 3.0T, using an endorectal coil and phased-array surface coil,[14] followed by robot-assisted laparoscopic radical prostatectomy. T1-weighted, T2-weighted, diffusion-weighted, dynamic contrast enhanced, and MR spectroscopy images were obtained, along with delayed axial post Gadolinium injection T1-weighted images of the abdomen.

A 9 × 7.5 mm hypointense lesion was detected in the right anterior central gland on T2W MRI and apparent diffusion coefficient (ADC) maps of DW MRI. MR spectroscopy revealed a voxel with increased choline/citrate ratio and DCE MRI demonstrated hyper-enhancement within the lesion, supporting the diagnosis of cancer (figure 1a-e). In addition there were right mid and bilateral mid-base peripheral zone lesions that were positive only on T2W MRI. There was no evidence for extracapsular extension, seminal vesicle invasion, nodal or osseous involvement.

Generation of Patient-Specific Prostate Mold, Specimen Processing and Correlation

Prior to the prostatectomy, a mold of the prostate based on the MR images was created. Design of the mold begins by manual segmentation of pre-surgical multiplanar T2W MR images of the prostate. The prostate is outlined in each MRI plane and converted via

$watermark-text

$watermark-text

$watermark-text

software into a 3D object that represents the topography of the patient's prostate. The 3D object is then compared back against the original MR images to resolve any discrepancies.

The final 3D model of the prostate is then imported into SolidWorks (SolidWorks, Dassault Systèmes SolidWorks Corp., Concord, MA, USA), a 3D design software. There, it is subtracted from a pre-generated rectangular mold to create an internal cavity that precisely shapes the patient's prostate based on the MRI. Slots for slicing the prostate are designed into the mold at 6 mm intervals corresponding with the location of the axial MR slices. To allow proper orientation of the patient's prostate, the mold is marked with labels for left, right, base, apex, and the cranial and caudal ends of the urethra. The mold is generated in two halves as shown (figure 2a) to allow insertion of the prostate specimen. The mold is printed using a 3D printer (Dimension Elite 3D printer, Stratasys, Inc., Eden Prarie, MN, USA) that deposits consecutive 0.010 inch layers of acrylonitrile butadiene styrene (ABS) plastic to create the final prostate mold (figure 2b). To reduce the amount of plastic needed, solid portions of the mold are printed in a honeycomb lattice.

After surgical excision, the prostate is transported to the pathology lab where the specimen is inked such that the anterior is black, right posterior is blue, left posterior is red, and urethra is yellow (figure 3a). The prostate is then fixed in formalin overnight at room temperature.

Prior to placing the prostate into the mold, the seminal vesicles are excised. The prostate is oriented in the mold such that the color-coding matches the labels on the mold (figure 3b). The dual urethral markers are important for appropriately rotating the specimen within the mold. Whole mount sections of the prostate are cut with a single long blade using the mold as a guide creating 6mm tissue blocks (figure 4). A single blade was chosen because it avoids the difficulties encountered with a multi-blade approach such as increased friction and specimen displacement.

After slicing, histopathologic sections were prepared from the tissue blocks and a Gleason 6 (3+3) lesion was identified in the right anterior central gland (figure 1f). The size and location of the lesion correlated with the findings on multiparametric MR imaging previously described. The patient-specific mold allowed for direct histopathologic correlation with the MRI findings, validating the ability of MRI to detect prostate cancer in this case.

Comment (Peter Pinto, MD)

Anterior lesions such as the one seen in this patient are difficult to detect on DRE and can easily be missed on TRUS guided biopsy. In these cases, MR imaging may prove to be an invaluable diagnostic tool in a urologist's armamentarium, however its accuracy still requires further validation. Prior studies have attempted to define various techniques of specimen orientation, securing, and sectioning to register tumor locations between histopathology and MR imaging. [23] Graser et al. divided the entire prostate into six segments (right and left bases, middle gland, and apex) and correlated histopathologic findings in each sextant to gross regions on MRI.[16] Kiessling et al. generated 3D reconstructions of histologic images, which could then be digitally re-sliced in similar planes to MRI.[17] Fütterer et al. considered histopathology findings to match MRI if located within 8 mm, or two slices.[18] Several groups have also constructed devices to hold the prostate during slicing, however none of these devices conform to the *in vivo* shape of the patient's prostate during MRI nor do they control for prostate deformation during slicing.[19–21] Our previous method of correlation without a patient-specific mold lacked strict one to one registration between the MRI and corresponding whole mount sections.[14] Our current technique overcomes this issue by offering the advantage of combining gross anatomic

$watermark-text

$watermark-text

$watermark-text

landmarks with *in vivo* MRI measurements for orientation, a patient-specific mold to secure and reshape the organ during slicing, and slots of equal spacing for controlling section angle and thickness. We have shown that this technique can be used to accurately register histopathologic images to MR imaging findings, a crucial step in validating MRI as a tool for diagnosis and localization of prostate cancer.

The prostate mold defined in our report is not without its limitations. The initial cost of the 3D printer is nearly $15,000 while the cost of the ABS plastic per mold is $80. Generating the mold is also time consuming as it currently requires manual segmentation of the area of interest from the pre-surgical MRI and approximately 8 hours to print. This necessitates advanced planning and could limit the frequency of patients for whom this technique can be applied. We also observed that in cases where the prostate was removed with excess surrounding tissue (i.e. periprostatic fat), fitting the prostate into the mold was difficult. Finally, although this customized prostate mold has proven to be a valuable tool for research, its applications to community practice are limited at this time. In the future, it is anticipated that the speed of printing could be optimized, and cost reduced to less than $10 by using less expensive material. Furthermore, lower cost entry-level printers (<$4,000) are available which print faster at lower resolutions, albeit still seemingly adequate for our prostate mold application. We are also investigating slicing the prostate while fresh instead of fixed to enable biomolecular profiling (i.e. genomics). We hope these advances will play a role in enabling individually tailored focal therapies in the future.

Conclusion

The ability to use MRI as a means to localize and stage a patient's prostate cancer has the potential to improve its diagnosis and management. Newer prostate biopsy techniques that are in gantry or those that fuse a patient's MRI with TRUS guided platforms can be used to obtain targeted biopsy samples rather than blind biopsies, which may fail to detect a patient's cancer or undersample it.[7] Once a region of cancer has been identified, these patients may go on to receive targeted therapy rather than treatment of the entire gland, thus decreasing the potential for significant morbidity.[6] These advances will be dependent on the further development and refinement of imaging modalities such as MRI as an accurate tool in identifying, localizing, and staging prostate cancer. To this end, our patient-specific MRI based prostate mold allows for the precise validation of *in vivo* imaging studies by enabling registration to whole mount histopathology.

References

1. American Cancer Society. Cancer Facts & Figures 2010. Atlanta: American Cancer Society; 2010.
2. Levine MA, Ittman M, Melamed J, Lepor H. Two consecutive sets of transrectal ultrasound guided sextant biopsies of the prostate for the detection of prostate cancer. J Urol. 1998; 159:471–476. [PubMed: 9649265]
3. Djavan B, Waldert M, Zlotta A, Dobronski P, Seitz C, Remzi M, Borkowski A, Schulman C, Marberger M. Safety and morbidity of first and repeat transrectal ultrasound guided prostate needle biopsies: Results of a prospective european prostate cancer detection study. J Urol. 2001; 166:856–860. [PubMed: 11490233]
4. Rifkin MD, Zerhouni EA, Gatsonis CA, Quint LE, Paushter DM, Epstein JI, Hamper U, Walsh PC, McNeil BJ. Comparison of magnetic resonance imaging and ultrasonography in staging early prostate cancer. results of a multi-institutional cooperative trial. N Engl J Med. 1990; 323 :621–626. [PubMed: 2200965]
5. Norberg M, Egevad L, Holmberg L, Sparén P, Norlén BJ, Busch C. The sextant protocol for ultrasound-guided core biopsies of the prostate underestimates the presence of cancer. Urology. 1997; 50:562–566. [PubMed: 9338732]

$watermark-text

$watermark-text

$watermark-text

6. Xu S, Kruecker J, Turkbey B, Glossop N, Singh AK, Choyke P, Pinto P, Wood BJ. Real-time MRI-TRUS fusion for guidance of targeted prostate biopsies. Computer Aided Surgery. 2008; 13:255–264. [PubMed: 18821344]
7. Turkbey B, Pinto PA, Choyke PL. Imaging techniques for prostate cancer: implications for focal therapy. Nat Rev Urol. 2009; 6(4):191–203. [PubMed: 19352394]
8. Fütterer JJ, Heijmink SWTPJ, Scheenen TWJ, Veltman J, Huisman HJ, Vos P, Hulsbergen-Van De Kaa CA, Witjes JA, Krabbe PFM, Heerschap A, Barentsz JO. Prostate cancer localization with dynamic contrast-enhanced MR imaging and proton MR spectroscopic imaging. Radiology. 2006; 241:449–458. [PubMed: 16966484]
9. Miao H, Fukatsu H, Ishigaki T. Prostate cancer detection with 3-T MRI: Comparison of diffusion-weighted and T2-weighted imaging. Eur J Radiol. 2007; 61:297–302. [PubMed: 17085002]
10. Delongchamps NB, Rouanne M, Flam T, Beuvon F, Liberatore M, Zerbib M, Cornud F. Multiparametric magnetic resonance imaging for the detection and localization of prostate cancer: combination of T2-weighted, dynamic contrast-enhanced and diffusion-weighted imaging. BJU International. 2010 [in press].
11. Reinsberg SA, Payne GS, Riches SF, Ashley S, Brewster JM, Morgan VA, DeSouza NM. Combined use of diffusion-weighted MRI and 1H MR spectroscopy to increase accuracy in prostate cancer detection. Am J Roentgenol. 2007; 188:91–98. [PubMed: 17179350]
12. Engelbrecht MR, Huisman HJ, Laheij RJF, Jager GJ, Van Leenders GJLH, Hulsbergen-Van De Kaa CA, De la Rosette JJMCH, Blickman JG, Barentsz JO. Discrimination of prostate cancer from normal peripheral zone and central gland tissue by using dynamic contrast-enhanced MR imaging. Radiology. 2003; 229:248–254. [PubMed: 12944607]
13. Choi YJ, Kim JK, Kim N, Kim KW, Choi EK, Cho KS. Functional MR imaging of prostate cancer. Radiographics. 2007; 27:63–75. [PubMed: 17234999]
14. Turkbey B, Pinto PA, Mani H, Bernardo M, Pang Y, McKinney YL, Khurana K, Ravizzini GC, Albert PS, Merino MJ, Choyke PL. Prostate cancer: Value of multiparametric MR imaging at 3 T for detection - histopathologic correlation. Radiology. 2010; 255:89–99. [PubMed: 20308447]
15. Heijmink SWTPJ, Fütterer JJ, Hambrock T, Takahashi S, Scheenen TWJ, Huisman HJ, Hulsbergen Van De Kaa CA, Knipscheer BC, Kiemeney LALM, Witjes JA, Barentsz JO. Prostate cancer: Body array versus endorectal coil MR imaging at 3T - comparison of image quality, localization, and staging performance. Radiology. 2007; 244:184–195. [PubMed: 17495178]
16. Graser A, Heuck A, Sommer B, Massmann J, Scheidler J, Reiser M, Mueller-Lisse U. Per-sextant localization and staging of prostate cancer: Correlation of imaging findings with whole-mount step section histopathology. Am J Roentgenol. 2007; 188:84–90. [PubMed: 17179349]
17. Kiessling F, Le-Huu M, Kunert T, Thorn M, Vosseler S, Schmidt K, Hoffend J, Meinzer H, Fusenig NE, Semmler W. Improved correlation of histological data with DCE MRI parameter maps by 3D reconstruction, reslicing and parameterization of the histological images. Eur Radiol. 2005; 15:1079–1086. [PubMed: 15747142]
18. Fütterer JJ, Heijmink SWTPJ, Scheenen TWJ, Jager GJ, Hulsbergen-Van De Kaa CA, Witjes JA, Barentsz JO. Prostate cancer: Local staging at 3-T endorectal MR imaging - early experience. Radiology. 2006; 238:184–191. [PubMed: 16304091]
19. Jhavar SG, Fisher C, Jackson A, Reinsberg SA, Dennis N, Falconer A, Dearnaley D, Edwards SE, Edwards SM, Leach MO, Cummings C, Christmas T, Thompson A, Woodhouse C, Sandhu S, Cooper CS, Eeles RA. Processing of radical prostatectomy specimens for correlation of data from histopathological, molecular biological, and radiological studies: A new whole organ technique. J Clin Pathol. 2005; 58:504–508. [PubMed: 15858122]
20. Ma HY, Phee L, Thng CH, Tan PH, Yuen J, Ng WS, Cheng C. A Novel Device for Sectioning Prostate in Correlation to MRI. The IASTED International Conference on Biomechanics. BioMech. 2004:156–161.
21. Jackson ASN, Reinsberg SA, Sohaib SA, Charles-Edwards EM, Jhavar S, Christmas TJ, Thompson AC, Bailey MJ, Corbishley CM, Fisher C, Leach MO, Dearnaley DP. Dynamic contrast-enhanced MRI for prostate cancer localization. Br J Radiol. 2009; 82:148–156. [PubMed: 19168692]

22. Shah V, Pohida T, Turkbey B, Mani H, Merino M, Pinto PA, Choyke P, Bernardo M. A method for correlating in vivo prostate magnetic resonance imaging and histopathology using individualized magnetic resonance-based molds. Rev Sci Instrum. 2009; 80:104301. [PubMed: 19895076]

23. Chen LH, Ho H, Lazaro R, Thng CH, Yuen J, Ng WS, Cheng C. Optimum slicing of radical prostatectomy specimens for correlation between histopathology and medical images. Int J Comput Assist Radiol Surg. 2010; 5:471–487. [PubMed: 20180036]

$watermark-text

$watermark-text

$watermark-text

$watermark-text
$watermark-text
$watermark-text

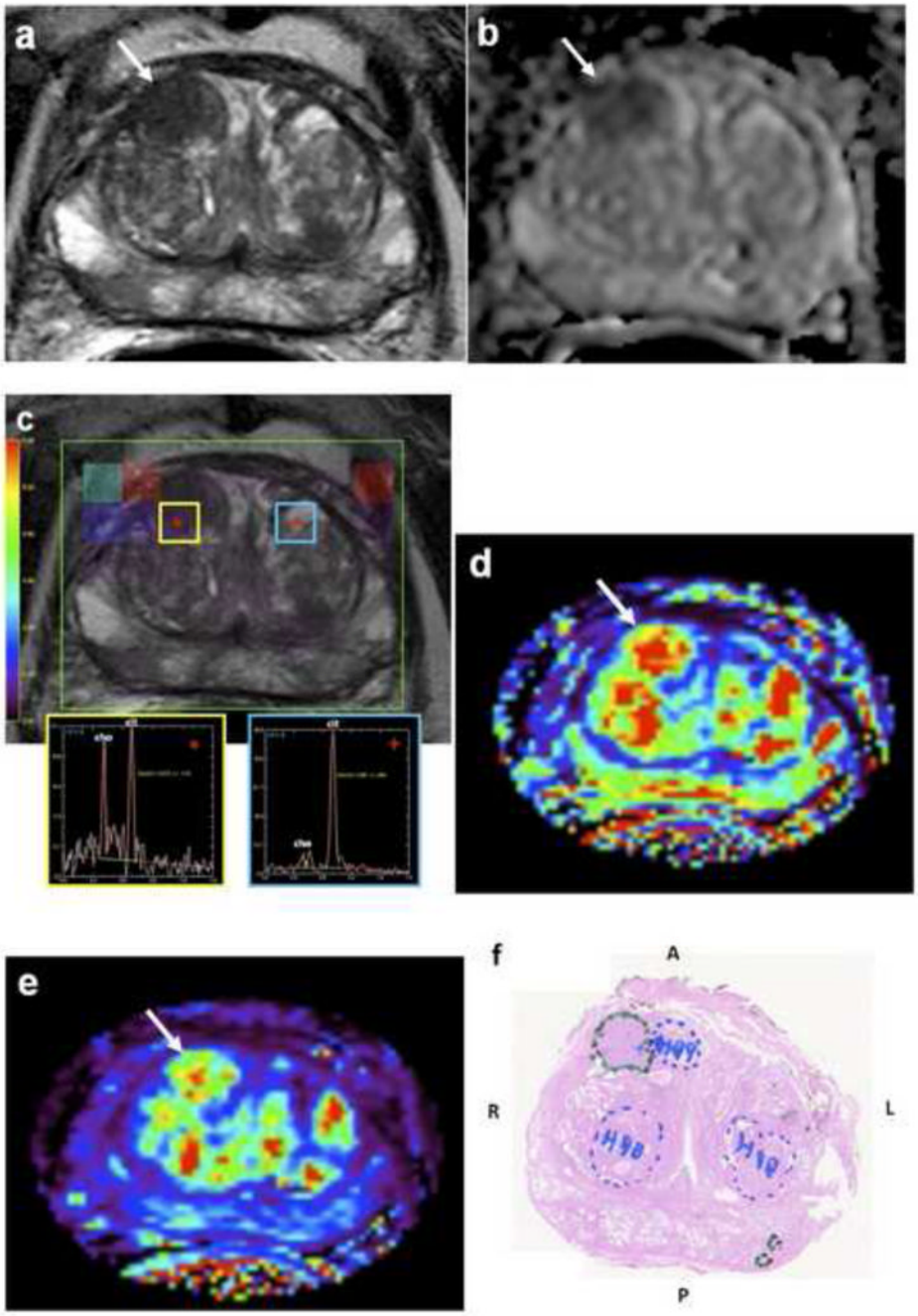

Figure 1.

Prostate multiparametric MRI and whole mount histopathology correlation. Axial T2-weighted **(a)** and ADC map of diffusion weighted **(b)** MR images demonstrate a hypointense lesion (arrow) in right mid anterior central gland suspicious for cancer. MR spectroscopy **(c)** increases the suspicion for cancer by demonstrating an increased ratio of choline *(cho)* to citrate *(cit)* ratio in this right mid anterior central gland lesion (*) when compared with the normal adjacent left side (+). Forward contrast rate [K^{trans}] **(d)** and reverse contrast rate [k_{ep}] **(e)** maps of dynamic contrast enhanced MRI support presence of tumor (arrow). Histopathologic whole mount slide **(f)** confirms presence of Gleason score

3+3=6 cancer (green dotted line), correlating to the tumor detected on multi-parametric MRI (*A* = anterior, *L* = left, *P* = posterior, *R* = right). Areas outlined in blue represent BPH.

$watermark-text
$watermark-text
$watermark-text

$watermark-text
$watermark-text
$watermark-text

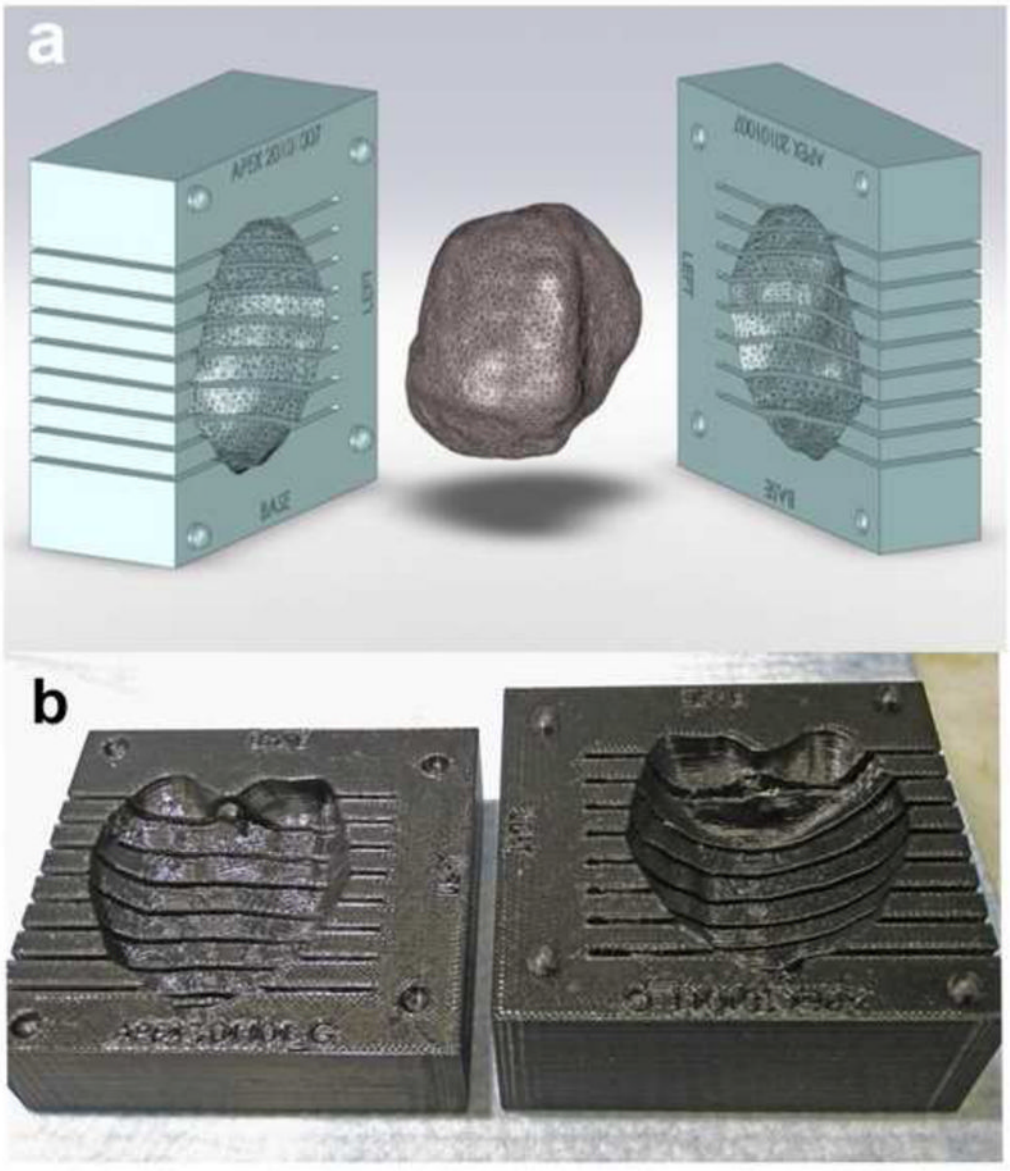

Figure 2.

Customized, patient-specific prostate specimen mold. **(a)** Three-dimensional representation of final prostate mold in green, shown in two halves with a 3D model of the patient's prostate shown in brown. The mold is labeled with the anatomic boundaries of the prostate (base, apex, left) and two markers for either side of the urethra. Slots placed every 6 mm on the mold correspond anatomically with location of MR axial slices, allowing the prostate to be sectioned such that histologic sections can be registered with MR images. **(b)** Mold is created using a 3D printer, shown here in two halves fit together using small pegs/slots in the corners.

$watermark-text
$watermark-text
$watermark-text

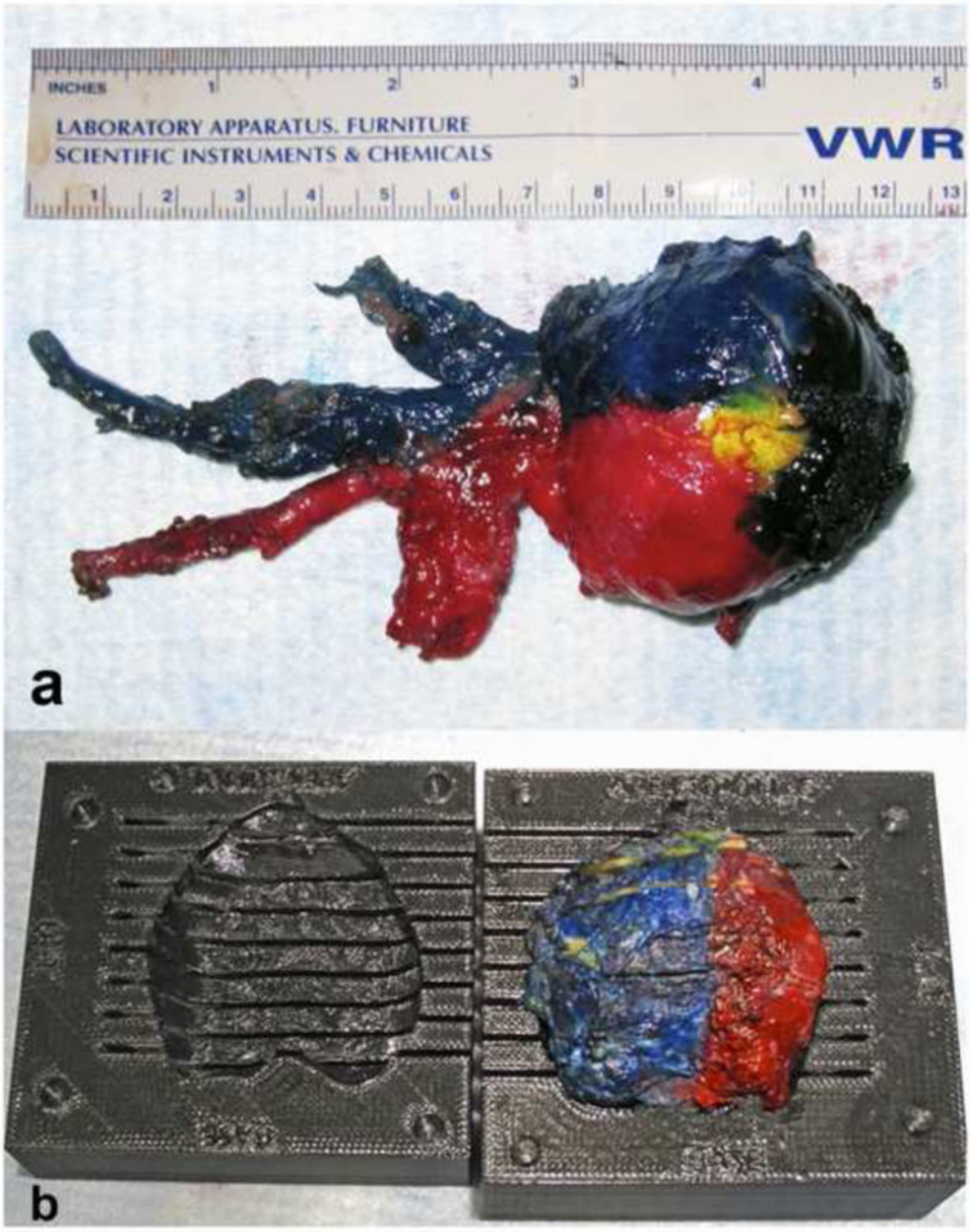

Figure 3.
Excised prostate specimen. **(a)** Specimen shown immediately following excision with seminal vesicles attached, inked as follows to maintain orientation: anterior black, right posterior blue, left posterior red, and urethra yellow. **(b)** After overnight formalin fixation, seminal vesicles are excised and specimen is placed in the mold with the appropriate orientation, prior to being closed and sectioned.

$watermark-text
$watermark-text
$watermark-text

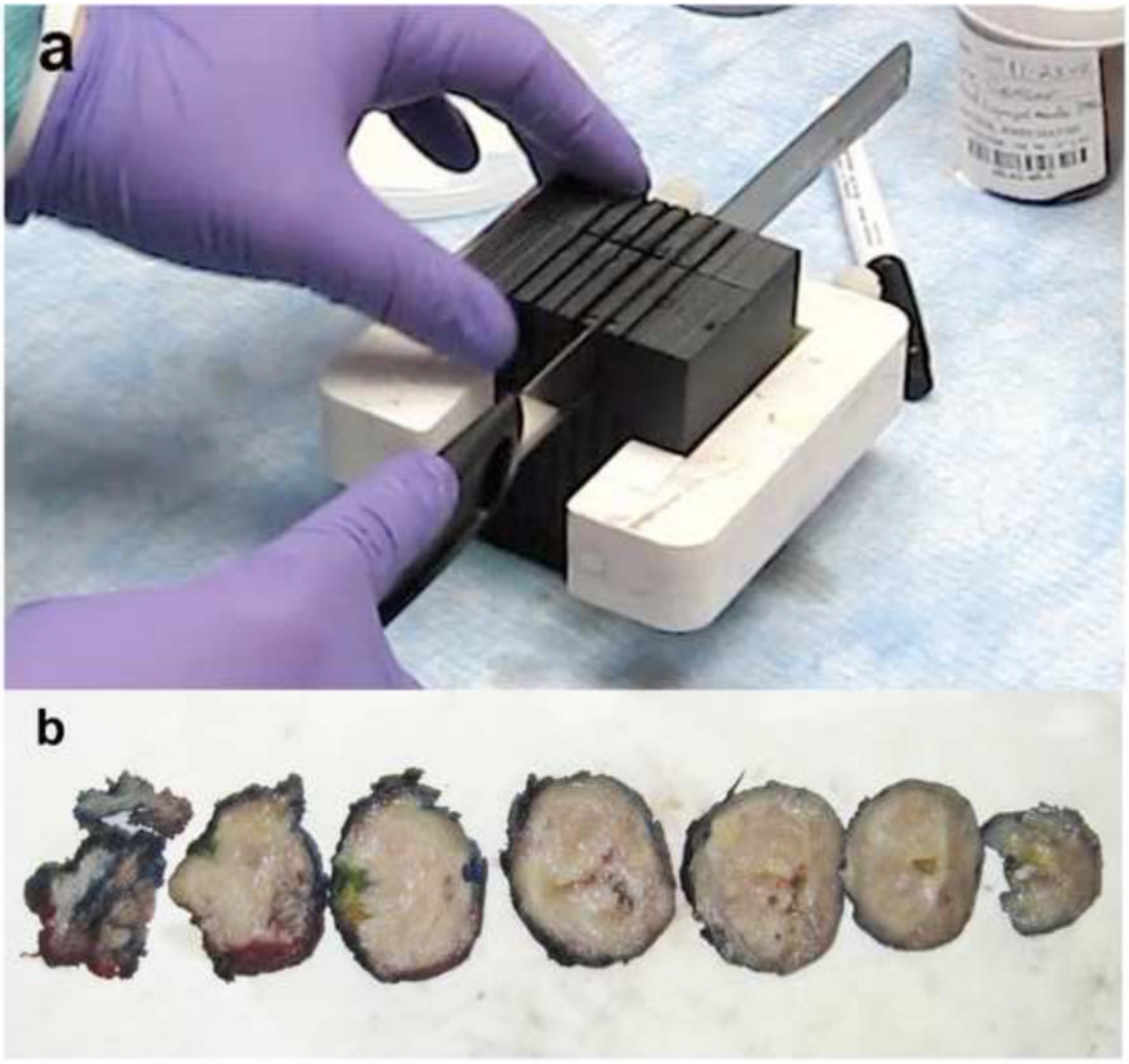

Figure 4.

Prostate slicing within the mold and resultant tissue blocks. **(a)** Mold is closed and clamped to prevent motion or significant tissue deformation while slicing. **(b)** Resultant 6 mm tissue blocks, arranged from base to apex, are used to create whole mount histopathology slides. These slides can then be correlated 1 to 1 with their corresponding axial MRI slices.